Journal Pre-proof

Cytosine deaminase base editing to restore *COL7A1* in dystrophic epidermolysis bullosa human:murine skin model.

G. Naso, S.A. Gkazi, C. Georgiadis, V. Jayarajan, J. Jacków, R. Fleck, L. Allison, O.K. Ogunbiyi, J.A. McGrath, D. Ilic, W.L. Di, A. Petrova, W. Qasim

PII: S2667-0267(23)00013-9

DOI: https://doi.org/10.1016/j.xjidi.2023.100191

Reference: XJIDI 100191

To appear in: *JID Innovations*

Received Date: 6 April 2022

Revised Date: 26 December 2022

Accepted Date: 6 January 2023

Please cite this article as: Naso G, Gkazi S, Georgiadis C, Jayarajan V, Jacków J, Fleck R, Allison L, Ogunbiyi O, McGrath J, Ilic D, Di W, Petrova A, Qasim W, Cytosine deaminase base editing to restore *COL7A1* in dystrophic epidermolysis bullosa human:murine skin model., *JID Innovations* (2023), doi: https://doi.org/10.1016/j.xjidi.2023.100191.

Cytosine deaminase base editing to restore *COL7A1* in dystrophic epidermolysis bullosa human:murine skin model.

Naso G[1], Gkazi SA[1], Georgiadis C[1], Jayarajan V[1], Jacków J[2], Fleck R[3], Allison L[3], Ogunbiyi OK[4], McGrath JA[2], Ilic D[5], Di WL[1], Petrova A[1]* and Qasim W[1].

[1] Molecular and Cellular Immunology Unit, UCL GOS Institute of Child Health, 30 Guilford Street, London, WC1N 1EH, UK.
[2] St John's Institute of Dermatology, Kings College London (Guy's Campus), Great Maze Pond, London, SE1 9RT, UK.
[3] Centre for Ultrastructural Imaging, King's College London, London, SE1 1UL UK.
[4] UCL Great Ormond Street Institute of Child Health, Department of Histopathology, Camelia Botnar Laboratories, Level 3, London, WC1N 3JH
[5] Department of Women and Children's Health, School of Life Course Sciences, Faculty of Life Sciences and Medicine, King's College London, London, SE1 9RT, UK.
*Corresponding author e-mail: petrova.anastasia@gmail.com

ORCiDs

Naso, Gaetano https://orcid.org/0000-0002-7664-7260

Gkazi, Soragia Athina https://orcid.org/0000-0002-6385-368X

Georgiadis, Christos https://orcid.org/0000-0003-0031-8396

Jayarajan, Vignesh https://orcid.org/0000-0002-1185-3274

Jacków, Joanna https://orcid.org/0000-0002-5744-7896

Fleck, Roland https://orcid.org/0000-0003-1542-6218

Allison, Leanne https://orcid.org/0000-0003-2954-9892

Ogunbiyi, Olumide Kayode https://orcid.org/0000-0001-5208-5526

McGrath, John Alexander https://orcid.org/0000-0002-3708-9964

Ilic, Dusko https://orcid.org/0000-0003-1647-0026

Di, Wei-Li https://orcid.org/0000-0002-4851-1649

Petrova, Anastasia https://orcid.org/0000-0001-5294-399X

Qasim, Waseem https://orcid.org/0000-0001-8353-4494

ABSTRACT

Recessive dystrophic epidermolysis bullosa (RDEB) is a debilitating blistering skin disorder caused by loss-of-function mutations in *COL7A1* encoding type VII collagen (C7), the main component of anchoring fibrils (AFs) at the dermal-epidermal junction (DEJ). Although conventional gene therapy approaches through viral vectors have been tested in pre-clinical and clinical trials, they are limited by transgene size constraints and only support unregulated gene expression. Genome editing could potentially overcome some of these limitations, and CRISPR/Cas9 has already been applied in research studies to restore *COL7A1* expression. Delivery of suitable repair templates for repair of DNA cleaved by Cas9 is still major challenge, and alternative base editing strategies may offer corrective solutions for certain mutations.

We demonstrate highly targeted and efficient cytidine deamination and molecular correction of a defined RDEB mutation (c.425A>G) leading to restoration of full-length C7 protein expression in primary human fibroblasts and iPSCs. C7 basement membrane expression and skin architecture were restored with *de novo* AFs identified by electron microscopy in base edited human RDEB grafts recovered from immunodeficient mice. The results demonstrate the potential and promise of emerging base editing technologies in tackling inherited disorders with well-defined single nucleotide mutations.

INTRODUCTION

Recessive dystrophic epidermolysis bullosa (RDEB) is a severe genodermatosis caused by loss-of-function mutations in the *COL7A1* gene, which encodes for type VII collagen (C7) protein (Has et al., 2020). C7 is a key constituent of anchoring fibrils (AF) at the dermal-epidermal junction (DEJ), and its impairment compromises the integrity of the DEJ, leading to severe sublamina densa blistering and tissue cleavage (Burgeson, 1993). Currently clinical management for RDEB is limited to supportive care, including daily dressings and meticulous wound care combined with nutritional supplements (Fine and Mellerio, 2009a, 2009b, Grocott et al., 2013).

Various therapeutic strategies have been investigated for the treatment of RDEB (Angelis et al., 2016, Hou et al., 2021, Naso and Petrova, 2020, Natsuga et al., 2021). These included intradermal (Remington et al., 2009, Woodley et al., 2004) and systemic (Woodley et al., 2013) injection of recombinant C7, intradermal injection of allogeneic fibroblasts (Petrof et al., 2013, Venugopal et al., 2013), hematopoietic stem cell (HCT) transplantation (Tolar and Wagner, 2012, Wagner et al., 2010) and infusion of allogeneic mesenchymal stromal cells (MSCs) (Conget et al., 2010, Petrof et al., 2015). Recently, topical application of a HSV derived vector encoding C7 has shown promise in clinical trials, although repeated applications were required (Gurevich et al., 2022).

In addition, several *ex vivo* gene therapy approaches using vector modified fibroblasts or keratinocytes have shown promising results in pre-clinical and clinical settings (2014, Droz-Georget Lathion et al., 2015, Jackow et al., 2016, Latella et al., 2017, Lwin et al., 2019, Siprashvili et al., 2016), and no mutagenesis has been reported in these studies and trials to date.

Genome editing strategies, however, can be used to mediate precise, locus-specific correction of disease-causing mutations (Anzalone et al., 2020, Cox et al., 2015, Ran et al., 2013). Canonical CRISPR/Cas9 system relies on the introduction of double stranded DNA breaks (DSBs) that are resolved *via* either non-homologous end joining (NHEJ) or homology-directed repair (HDR). NHEJ typically produces small insertions and deletions (indels), and can be used to restore *COL7A1* expression through exon skipping and gene re-framing (Bonafont et al., 2019, Kocher et al., 2020, Takashima et al., 2019). HDR pathway, on the other hand, can be exploited to restore endogenous *COL7A1* sequence by introducing a donor template (Hainzl et al., 2017, Izmiryan et al., 2018, Jackow et al., 2019, Kocher et al., 2021, Webber et al., 2016). However, the low efficiency of this pathway in therapeutically relevant cells and the presence of accompanying NEJ events and potentially deleterious indels often requires antibiotic resistance cassettes or single cell selection to enrich for the corrected clones (Hainzl et al., 2017, Jackow et al., 2019, Webber et al., 2016).

In contrast, base editing tools involve DSB-free site-specific modifications mediating either C-G to T-A (cytosine base editor, CBE) or A-T to G-C (adenine base editor, ABE) conversions without double stranded DNA cleavage or exogenous donor template (Gaudelli et al., 2017, Komor et al., 2016, Komor et al., 2017, Rees and Liu, 2018). In addition, base editing is able to correct single nucleotide mutations with sufficient efficiency without the need for positive selection of gene corrected cells. In DEB, approximately 76% of registered mutations are single nucleotide mutations (Naso and Petrova, 2019) and up to 61% of those can potentially be corrected with CBE or ABE. Recently, ABE-mediated base editing was successfully demonstrated in primary RDEB fibroblasts and induced pluripotent stem cells (iPSCs) for two different *COL7A1* nonsense mutations (Osborn et al., 2020).

In this study, we investigated the potential of CBE-mediated correction of a known mutation in primary fibroblasts and patient-derived iPSCs. The splice-site mutation 425A>G, at exon 3 of

COL7A1, is a frequent mutation detected in various patient cohorts (Kern et al., 2006, Murata et al., 2004). We used 3rd generation human codon optimized base editor CBE3 mRNA and sgRNA to target this pathogenic mutation. Efficient and specific nucleotide correction in patient iPSCs and primary fibroblasts was observed, leading to the restoration of C7 expression *in vitro*. Crucially, base edited fibroblasts were able to restore the DEJ integrity by forming *de novo* AFs in human:murine chimeric skin graft mouse model *in vivo.*

RESULTS

Efficient base conversion in primary RDEB fibroblasts and iPSCs.

mRNA for CBE3 base editor was synthesized from plasmid containing coCBE3 (Figure 1a). Specific sgRNA (x3C7-CyD) was designed so that the c.425A>G mutation is optimally located within the 5bp CBE3 editing window at position C5 (Figure 1b). Sanger sequencing was used to confirm the presence of the c.425A>G mutation hotspot in both primary fibroblasts and iPSCs (Figure 1b). CoCBE3 mRNA and sgRNA were delivered into primary fibroblasts and iPSCs generated from the patient's cells harboring a homozygous c.425A>G mutation in *COL7A1* by electroporation. Patient iPSCs were differentiated into keratinocyte-like lineages to assess protein restoration *in vitro*, while the fibroblasts were used to assess functional recovery *in vivo* (Figure 1c). Patient-derived iPSCs expressed the markers of pluripotency as assessed by immunofluorescence and flow cytometry and were able to differentiate towards all three germ layers in a trilineage differentiation assay (Figure 2).

Sanger sequencing-based EditR analysis of the DNA from the treated cells revealed up to 61% and 45% of targeted C>T (G>A) base conversion at the desired c.425 (C5) position in patient fibroblasts and iPSCs, respectively (Figure 3a). Bystander C>T conversion at position c.426 (C4) was detected in 8% and 4% of Sanger sequencing reads in patient fibroblasts and iPSCs, respectively. The frequencies detected by Sanger sequencing analysis were further corroborated

by on-target next generation sequencing (NGS) analysis. On-target C>T conversion at position c.425/C5 was confirmed in over 51% and 59% of the reads for base edited iPSCs and fibroblasts, respectively (Figure 3b). As initially observed by Sanger sequencing, NGS confirmed the presence of additional bystander on-target C>T conversion within the predicted coCBE3 editing window at position C4 (19.4% in iPSCs and 4.8% in fibroblasts) and outside the window at position C3 (3.9% and 1% in iPSCs and fibroblasts, respectively), C1 (7.4% in iPSCs only) and C12 (1% in patient iPSCs only). Additionally, a small frequency of non-canonical C>T conversions was also observed at the target c.425 site (5.5% C>A, 6.6% C>G in iPSCs and 2.2% C>A, 2.7% C>G in fibroblasts). In total, changes within the sequencing window other than the desired C5 conversion totalled 42.9% for iPSCs and 11.7% for fibroblasts, indicating the need for further improvements.

To determine the frequency of C>T correction at position c.425 alone, haplotype-based analysis of the NGS data was carried out by CRISPResso2 (Clement et al., 2019) and revealed that up to 23.5% and 46% of reads harbored C>T changes at position c.425 only without the presence of unwanted bystander effects in patient iPSCs and fibroblasts, respectively (Figure 3c).

To exclude NHEJ effects due to possible residual nicking activity of the nCas9(D10A) within coCBE3 editing window (Komor et al., 2016), the presence of indels was evaluated by NGS. A small percentage of indels (3.6%; 2.5% deletions + 1.1% insertions) were detected in the target *COL7A1* sequence recognized by x3C7-CyD sgRNA.

Base editing resulted in a very low frequency of 'off-target' guide dependent events

To assess whether coCBE3 created off-target C>T editing in a guide-dependent fashion, the Benchling *in silico* predictive algorithm was used to identify the off-target regions that could potentially be targeted by the x3C7-CyD sgRNA protospacer (Figure 4a). The top 10 identified

off-target genomic loci were interrogated by NGS and off-target edits within coCBE3 editing window were detected at frequencies below 0.5% in 9 out of 10 off-target sites (Figure 4b). A 4% C>T change was detected at position 5 of the base editing window in 1 out of 10 evaluated sites (OT3) but was also present in untreated samples (p=0.25) so not attributed to base editing effects. A full list of C>T changes detected in the predicted off-target sites is detailed in Table 1.

With respect to possible NHEJ effects due to possible residual nicking activity of the nCas9(D10A) within coCBE3, no significant NHEJ activity was detected in the off-target sites when compared to untreated samples. (Figure 4c).

Base editing restores full-length C7 expression in primary RDEB fibroblasts and iPSC-derived keratinocyte like cells.

C7 expression in CBE3-edited RDEB fibroblasts was examined by immunostaining and immunoblotting. Positive C7 expression was detected in base edited cells but not in untreated patient cells (Figure 5a). Immunoblotting results showed that the presence of 290kDa band in base edited fibroblasts corresponding to full-length C7 protein from total cell lysate. (Figure 5b). Further, immunoblotting detected a full-length C7 in the cell culture supernatant harvested from base edited RDEB fibroblasts, indicating successful secretion of the protein (Figure 5c). Untreated patient cells and wild type fibroblasts were used as negative and positive controls of C7 expression, respectively. RDEB fibroblasts transduced with the lentiviral vector containing the full-length codon optimized *COL7A1* cDNA were used as an additional positive control (Georgiadis et al., 2016). To confirm restoration of C7 in coCBE3-edited iPSCs, the cells were differentiated into keratinocyte-like cells using a previously described protocol (Petrova et al., 2014). Immunofluorescent analysis confirmed the restoration of C7 expression in approximately 29.4% of base edited cells (Figure 5d). Importantly, iPSC-derived keratinocyte-

like cells displayed typical epidermal morphology and expression of epidermal stem cell markers, ΔNP63 and Keratin 14.

Base edited fibroblasts restore skin integrity *in human:murine skin grafts*

To determine whether base edited cells could result in deposition and incorporation of C7 into the DEJ, a human:murine xenograft skin model was adapted (Di et al., 2011, Di et al., 2012, Larcher et al., 2007). Bio-engineered skin grafts generated by base edited fibroblasts and untreated RDEB keratinocytes were grafted on NSG mice. Bio-engineered skin grafts incorporating untreated RDEB or healthy keratinocytes and fibroblasts were used as negative and positive controls, respectively.

Upon harvesting, the morphology of the grafts was evaluated by H&E staining and revealed multiple stratified epidermal layers in all conditions (Figure 6a). Blistering and splitting at the DEJ were observed in the grafts generated using untreated RDEB cells which closely resembled the human disease phenotype. On the contrary, no blistering was detected in the grafts generated using base edited fibroblasts or healthy fibroblasts. The human origin of the grafted area was confirmed by species-specific staining for mitochondrial marker (complex IV subunit II) to demarcate human:murine borders (Figure 6b). All grafts showed normal distributions of Keratin 14 and 10 in the basal and suprabasal epidermal layers, respectively (Figure 6c).

Base edited fibroblasts deposit C7 at the DEJ and form *de novo* AFs *in vivo*.

The restoration of integrity of the DEJ in the grafts was further confirmed by immunofluorescent analysis of C7 protein expression. No C7 was detected in the untreated RDEB grafts, while deposition of the protein at the DEJ was observed in the grafts containing base edited fibroblasts (Figure 7a and Figure 8a and c).

Importantly, transmission electron microscopy (TEM) was used to assess whether C7 expression in the grafts containing base edited fibroblasts translated to *de novo* AFs formation.

AFs were quantified by a well-established quantitative ultrastructural techniques in which AFs were counted along a 40-µm continuous stretch of the DEJ in a blinded fashion (Tidman and Eady, 1985). A blistering phenotype and extensive dermal-epidermal separation were observed in all RDEB grafts, with only 15-µm of unseparated skin available for evaluation in 2 of the three samples with mostly wispy, rudimentary AFs seen (Figure 7b and Figure 8b and d). On the contrary, the micrographs of the grafts containing base edited fibroblasts revealed an abundance of sub-lamina densa fibrillary structures that bore the ultrastructural characteristics of normal AFs exhibiting cross-banding and extending ~200 nm into the dermis, looping around type I and III dermal collagen fibers (Figure 7b). No blistering or tissue cleavage was observed at the DEJ, consistent with functional restoration of dermal-epidermal adhesion. AF quantification confirmed that a significantly (n=3, p=0.0002) higher number of AFs in the grafts containing base edited fibroblasts compared to untreated RDEB grafts (Figure 7c). These data clearly demonstrate that the base editing strategy not only led to restoration of C7 expression *in vivo* but also conferred functional correction of the DEJ through formation of *de novo* AFs.

DISCUSSION

This study investigated the potential of an early generation cytosine base editor to correct the known recurrent c.425A>G mutation within *COL7A1*. This splice-site mutation at position −2 at the donor splice site of exon 3 causes aberrant splicing of at least two abnormal transcripts, leading to a premature termination codon (PTC) downstream in the *COL7A1* gene. (Gardella et al., 1996, Hammami-Hauasli et al., 1997). Due to the proximity of the gene start, C7 protein expression and, hence, AFs are completely absent in patients homozygous for this mutation, often presenting with severe RDEB.

Genome editing promises to overcome the limitations of conventional gene addition approaches, especially for large transgenes. For RDEB-causative mutations, canonical CRISPR/Cas9-mediated correction through HDR relies on the efficient delivery of donor repair

template. Template delivery includes non-viral methods including plasmid DNA (Hainzl et al., 2017), double-stranded DNA (Webber et al., 2016), single-stranded oligonucleotides (Jackow et al., 2019), or viral based delivery (Izmiryan et al., 2018, Osborn et al., 2020).

Base editors, on the other hand, do not rely on the HDR pathway and hence alleviate the need for donor template delivery for the correction of single nucleotide mutations.

Furthermore, base editors delivered as mRNA, exhibit transient expression and have reduced risk of aberrant effects (Koblan et al., 2018, Rees and Liu, 2018). Recently, ABE delivery within virus-like retroviral particles was used to correct a RDEB mutation (Osborn et al., 2020), further demonstrating the adaptability of the platforms.

In our experiments, an early generation BE, BE3, combined D10A Cas9 nickase with rat APOBEC1 (rAPOBEC1) cytidine deaminase. This converts cytosine into uracil within a 5bp-catalytic window of activity between the 4th and the 8th base distal to the PAM on the non-target strand of the sgRNA (Komor et al., 2016). Uracil is subsequently converted to thymine during DNA replication or repair, while the inclusion of an inhibitor of uracil DNA glycosylase (UGI) prevents base excision repair. Subsequent iterations have employed additional UGI elements and improved fidelity to reduce the likelihood of indel creation, off-target effects and RNA deamination.

The c.425A>G mutation was amenable for CBE-mediated conversion given a pathogenic substitution is located at position 5 of the base editing window, albeit with an adjacent cytosine nucleotide. Co-delivery of the sgRNA and CoBE3 mRNA into primary fibroblasts and patient-derived iPSCs resulted in on target conversion rates of 61% and 45%, respectively. These results were confirmed through deep sequencing by NGS, where >59% and 51% of the targeted c.425A>G mutation correction was detected in patient iPSCs and fibroblasts, respectively. Importantly, bystander edits were detected at position C4 in 4.8% and 19.4% of NGS sequencing reads in patient fibroblasts and iPSCs, respectively. Computational predictions of

C>T changes indicated bystander edits at this position alone or in combination with the corrective edit may result in splicing aberrations involving partial or total exon 3 skipping, and/or activation of a cryptic splice donor site due to the alteration of a splice donor sequence in exon 3, similar to splicing aberrations previously reported in c.425A>G patients (Gardella et al., 1996). Importantly, NGS-based haplotype analysis of sequencing reads from patient fibroblasts confirmed that up to 46% of the cells contained the corrective C>T edit at the desired position alone without unwanted on-target events.

Overall, bystander edits both within and outside the editing window were more frequent in patient iPSCs compared to fibroblasts. In agreement with previous studies (Komor et al., 2016), C-to-non-T edits were also detected at low frequencies. As mentioned above, these effects may be addressed by next generation base editors with higher editing fidelity and specificity (Kim et al., 2017, Komor et al., 2017, Ma et al., 2016).

Off-target edits were also investigated by deep sequencing, and no appreciable base editing activity was observed in 9 out of 10 *in silico* predicted sites. The 4% substitution frequency at C5 in off-target 3 was present in controls and likely a naturally arising variant in cultured cells. It is worth noting that *in silico* off-target detection tools have predictive limitations (Chuai et al., 2018, Wilson et al., 2018). Unbiased, genome-wide approaches include *in vitro* cell-based methods with high throughput sequencing of genomic DNA (Doman et al., 2020) and include Digenome-seq (digested genome sequencing) (Kim et al., 2015). However, generation of CBE protein required for such examinations has proven problematic and assays screening for Cas9 nuclease effects (Cameron et al., 2017, Tsai et al., 2017, Tsai et al., 2015) have limited relevance. Nonetheless, NHEJ activity and indel formation due to the nicking of the non-edited strand is an important consideration with 3.5% NHEJ activity was detected in ‘on-target’ amplicons. Again, this is likely to be addressed by the inclusion of addition UGI elements in next generation editors. Our *in silico* predicted sites from Benchling were corroborated using

CRISPR RGEN Cas-OFFinder (Bae et al., 2014), CRISPRoff (Alkan et al., 2018) and CRISPOR (Concordet and Haeussler, 2018) algorithms. We were able to cross verify 8/10 of the sites interrogated by NGS across the four platforms. This type of predicted off-target analysis has quite major limitations and provides only a rudimentary analysis of guide-dependent effects, without accounting for guide-independent or promiscuous activity. Furthernore, RNA targeting by cytidine deaminases has also been described (Grunewald et al., 2019) albeit following transfection of base editor plasmids into a HEK 293T cell line. Delivery of codon-optimised base editor (CBE3) in the form of mRNA, as described here, may mitigate such concerns as a result of its transient expression within the cells. We have previously interrogated the possibility of promiscuous guide-independent C>N deamination of antigen specific receptor RNA collected from serial samples taken from primary human T cells edited with coBE3, with no evidence of RNA deamination compared to controls (Georgiadis et al., 2021, Preece et al., 2020).

Restoration of C7 protein expression in base edited fibroblasts was confirmed by immunofluorescence microscopy and western blotting. Importantly, western blotting using cell culture supernatant revealed the presence of full-length C7, indicating successful secretion of the protein. This translated to deposition of functional protein at the DEJ *in vivo* and formation of *de novo* AFs. Although C7 deposition was not continuous along the basement membrane zone, with patches devoid of immunofluorescent signal observed, ultrastructural analysis confirmed that the grafts engineered using base edited fibroblasts contained significantly higher number of AFs compared to untreated RDEB grafts, where extensive dermal-epidermal separation and blistering was observed. Although the number of AFs in grafts containing base edited fibroblasts was approximately half of that detected in healthy control grafts, this amount was sufficient to effectively repair epidermal-dermal adhesion and restore skin functionality. Previously it has been demonstrated approximately 10% of wild-type C7 levels is required for

AF formation and significant phenotype improvement in hypomorphic RDEB mouse models (Nystrom et al., 2013). A recent study demonstrated that skin equivalents composed of 11% and 15% CRISPR/Cas9-gene corrected keratinocytes and fibroblasts, respectively, resulted in 26% C7 re-expression and AF formation *in vivo* (Izmiryan et al., 2018).

Importantly, we were also able to successfully edit patient derived iPSCs and demonstrate restoration of protein expression in iPSC-derived keratinocyte-like cells by immunofluorescence. Since only a limited number of patient cells can be obtained from RDEB patient skin biopsies, iPSCs may in the future provide a source of material for autologous transplantation of therapeutically relevant cells, including fibroblasts, keratinocytes and mesenchymal stem cells (MSCs) (Itoh et al., 2013, Jackow et al., 2019, Webber et al., 2016).

Another recent study has demonstrated the feasibility of adenosine base editors for the correction of two RDEB causative mutations (Osborn et al., 2020). C7 protein restoration was confirmed in a 3D skin culture model *in vitro* and in a teratoma assay *in vivo*, where base edited iPSCs formed epithelial-like structures. However, C7 expression or AF formation was not examined in skin using a humanized animal model, as described here.

Overall, this report adds to the demonstration of the feasibility of base editing technology to correct *COL7A1* mutations and restore skin functionality through the formation of *de novo* AFs but also highlights limitations of early generation base editing tools. Ongoing improvements to narrow the base editing window, eliminate residual cleaving activity and minimise promiscuity may address these issues and provide novel therapeutic avenues for RDEB.

MATERIALS AND METHODS

Isolation and culture of primary fibroblasts.

Skin biopsies were obtained with authorization from the National Research Ethics Services, Westminster (07/H0802/104) and written informed consent. Fibroblasts homozygous for the c.425A>G mutation were isolated as previously described (Georgiadis et al., 2016) and cultured in DMEM supplemented with 10% FBS and 1% penicillin-streptomycin.

Reprograming of primary fibroblasts to iPSCs

Patient iPSC line was generated using the CytoTune™-iPS 2.0 Sendai Reprogramming (ThermoFisher Scientific, Massachusetts, USA) under feeder free conditions. The resultant colonies were cultured in TESR2 on laminin-511 coated plates at a concentration of 2.4µg/mL.

iPSC characterization

Antibodies used for iPSCs characterization are listed in the Table 4. For *in situ* immunofluorescence, cells were seeded onto sterile 13mm coverslips in a 24 well plate, cultured for 48 hours then fixed in 4% paraformaldehyde, blocked and permeabilized with 0.1% Triton X-100 3% BSA, and then incubated overnight at 4°C with the primary antibody, followed by incubation with secondary antibody and counterstaining with DAPI (4',6-Diamidino-2-Phenylindole). The coverslips were mounted on glass microscope glass with Prolong gold. Micrographs were imaged using a Zeiss observer 7 (Zeiss, Oberkochen, Germany) and processed using Image J (Wayne Rasband (NIH)).

For iPSCs characterization by flow cytometry, cells were incubated with the antibody at 4°C form 20 minutes for extracellular markers or were fixed in Fix & Perm® Medium A (ThermoFisher) for 20 minutes at room temperature, followed by incubation with the

antibody at 4°C for 1 hour in Fix & Perm® Medium B for intracellular markers. Cell acquisition was carried out on a 2-laser CyAn™ ADP Analyzer.

For pluripotency assessment on cDNA level, total RNA was extracted using RNeasy min kit (QIAGEN) and retro-transcribed using High-Capacity cDNA Reverse Transcription Kit (Thermofisher) according to manufacturer's instructions before PCR amplification.

Trilineage differentiation

To make embryoid bodies, undifferentiated cells were dissociated as single cell (day 0) with Accutase for 8 minutes at 37°C and seeded at high density in AggreWell™800. Cells were resuspended in EB formation medium (STEMCELLS technologies) supplemented with 10µM of HA-100 (STEMCELLS technologies) for 1 week (Day 7). iPSC aggregates were then transferred on Matrigel®-coated plates with coverslips and cultured in DMEM 10% FBS for 3 weeks. After differentiation, cells were fixed in PFA 4% and analysed by immunofluorescence for the expression of mesoderm, endoderm and ectoderm markers.

Directed differentiation of iPSCs into keratinocytes

Base edited iPSCs were differentiated into keratinocytes as previously described (Petrova et al., 2014).

CBE3-mediated base editing

x3C7-CyD sgRNA (CACCCTGGGGACACCAGGTC, antisense orientation) was designed using the online Benchling CRISPR design tool (https://benchling.com/crispr). Synthetic sgRNAs were manufactured by Synthego (California, USA) using automated solid-phase synthesis with 2'-O-methyl 3' phosphorothioate modifications in the first and last 3 nucleotides. Third generation CBE (CBE3) plasmid was human codon optimised and mRNA was custom synthesized by TriLink using proprietary CleanCap® technology to increase expression and

stability For the delivery of base editing reagents, $1x10^6$ cells were electroporated with 2µg of sgRNA and 5µg of co-CBE3 mRNA in 100µl cuvettes of 4D-Nucleofector™ X Unit using EN-150 or CA-137 program for fibroblasts and iPSCs, respectively. Cells were then cultured at 30°C for 24hrs before returning to 37°C culture conditions.

Assessment of CBE3-mediated activity

Seven days post-electroporation, DNA was extracted using DNeasy Blood & Tissue Kit (Qiagen) and PCR across the target site (Exon5-COL7A1-REV GGAACTCACGAGGTCGGGTC and Intron2-COL7A1-FWD CAGTGCAGTACAGCGATGACC) was performed using Q5® High-Fidelity DNA Polymerase master mix (New England, BioLabs). Purified PCR products were analysed using Sanger-sequencing-based EditR analysis.

Next generation sequencing for the assessment of on- and off-target events

Online software Benchling was used to predict top 10 *in silico* off-targets for the designed guide sequence (Table 2). NGS libraries for on- and off-target sites were prepared using a Nextera XT Kit (Illumina, Cambridge, UK). Products were amplified using combinations of target-specific primers (Table 3). After the library preparation, individually barcoded samples were pooled and run in MiSeq using a 500-V2 nano-cartridge. Demultiplexed fastq files were uploaded to Galaxy (Afgan et al., 2018) for quality check, trimming and alignment. Base conversions and NHEJ signatures were analyzed using Naïve Variant Caller and Pindel, respectively (Ye et al., 2009). Figures were created using GraphPad Prism.

Immunofluorescence and immunoblotting

Immunofluorescence and immunoblotting were performed as previously described (Petrova et al., 2020). Immunofluorescent detection was performed with a monoclonal C7 antibody (LH7.2 clone, Sigma-Aldrich), while a polyclonal anti-human C7 antibody (Chen et al., 2002) was used

for immunoblotting (Chen et al., 2002). A full list of antibodies used in this study is available in Table 4. Staining was visualized and imaged using a Zeiss Observer 7 and processed using ZEN pro software (Zeiss, Oberkochen, Germany). Post-processing and quantification was carried out using Fiji as previously described (Petrova et al., 2020). For immunoblotting, the total protein concentration was determined using Pierce™ 660nm Protein Assay (ThermoFisher) and equal quantities (65µg) of total protein were loaded on SDS-PAGE.

Bioengineered skin preparation and grafting on immunodeficient mice

The methods for preparing and grafting bioengineered skin on immunodeficient NOD-scid IL2Rgammanull mice have been described previously (Petrova et al., 2020). In brief, for the dermal compartment 1.5 $\times 10^5$ WT fibroblasts, untreated RDEB ((+/+) c.425A>G, p.Lys142Arg)) fibroblasts or base edited RDEB fibroblasts ((+/+) were used (n=3/each)). WT or RDEB keratinocytes were used for the epidermal compartment for WT or RDEB (both containing untreated and base edited fibroblasts) grafts, respectively. All animal studies were approved by the University College London Biological Services Ethical Review Committee and licensed under the Animals (Scientific Procedures) Act 1986 (Home Office, London, United Kingdom).

Transmission electron microscopy

Sample processing for TEM was performed as previously described (Georgiadis et al., 2016). Images were acquired with JEOL JEM 1400 Plus TEM with a JEOL Ruby CCD camera (JEOL, Welwyn Garden City, UK). Consecutive 40 overlapping images covering 40-µm of a well-defined lamina densa taken at x15k magnification in a blinded fashion, where the identity of the samples was unknown during imaging and AF quantification and unblinded only after those were completed. AF scoring was performed using established quantitative ultrastructural

techniques (Tidman and Eady, 1985). Student's t-test was used to carry out the statistical analysis.

DATA AVAILABILITY STATEMENT

The NGS dataset related to this article can be found at https://submit.ncbi.nlm.nih.gov/subs/bioproject, hosted at BioProject NCBI repository. BioProject ID is PRJNA906066. Other datasets necessary to interpret and or replicate data in this paper are available upon request to the corresponding author.

CONFLICT OF INTERESTS

The authors state no conflict of interest.

ACKNOWLEDGEMENTS

This work was supported by CureEB, NIHR (Grant Ref:RP-2014-05-007), GOSH-ICH BRC and MRC (Grant Ref: MR/S036989). For the purpose of open access, the author has applied a Creative Commons Attribution (CC BY) licence to any Author Accepted Manuscript version arising. The views expressed are those of the authors and not necessarily those of the NHS, the NIHR, or the Department of Health. The authors acknowledge Microscopy and Flow Cytometry Core Facilities at UCL GOSH ICH and the staff at Biological Services Animal Facility.

AUTHOR CONTRIBUTIONS STATEMENT

Conceptualization: GN, WQ, AP; Methodology: GN, SAG, CG, JJ, ID, WLD, WQ, AP; Formal Analysis: GN, SAG, AP; Funding Acquisition: JAM, WQ, AP, WLD; Investigation: GN, SAG, CG, VJ, JJ, LA, OKO, DI, AP; Resources: SAG, OKO, RF, LA, ID, JAM, WLD, WQ; Writing: GN, CG, JJ, WLD, JAM, WQ, AP.

REFERENCES

Phase I/II ex vivo gene therapy clinical trial for recessive dystrophic epidermolysis bullosa using skin equivalent grafts genetically corrected with a COL7A1-encoding SIN retroviral vector (GENEGRAFT). Hum Gene Ther Clin Dev 2014;25(2):65-6.

Afgan E, Baker D, Batut B, van den Beek M, Bouvier D, Cech M, et al. The Galaxy platform for accessible, reproducible and collaborative biomedical analyses: 2018 update. Nucleic Acids Res 2018;46(W1):W537-W44.

Alkan F, Wenzel A, Anthon C, Havgaard JH, Gorodkin J. CRISPR-Cas9 off-targeting assessment with nucleic acid duplex energy parameters. Genome Biol 2018;19(1):177.

Angelis A, Kanavos P, Lopez-Bastida J, Linertova R, Oliva-Moreno J, Serrano-Aguilar P, et al. Social/economic costs and health-related quality of life in patients with epidermolysis bullosa in Europe. Eur J Health Econ 2016;17 Suppl 1:31-42.

Anzalone AV, Koblan LW, Liu DR. Genome editing with CRISPR-Cas nucleases, base editors, transposases and prime editors. Nat Biotechnol 2020;38(7):824-44.

Bae S, Park J, Kim JS. Cas-OFFinder: a fast and versatile algorithm that searches for potential off-target sites of Cas9 RNA-guided endonucleases. Bioinformatics 2014;30(10):1473-5.

Bonafont J, Mencia A, Garcia M, Torres R, Rodriguez S, Carretero M, et al. Clinically Relevant Correction of Recessive Dystrophic Epidermolysis Bullosa by Dual sgRNA CRISPR/Cas9-Mediated Gene Editing. Mol Ther 2019;27(5):986-98.

Burgeson RE. Type VII collagen, anchoring fibrils, and epidermolysis bullosa. J Invest Dermatol 1993;101(3):252-5.

Cameron P, Fuller CK, Donohoue PD, Jones BN, Thompson MS, Carter MM, et al. Mapping the genomic landscape of CRISPR-Cas9 cleavage. Nat Methods 2017;14(6):600-6.

Chen M, Costa FK, Lindvay CR, Han YP, Woodley DT. The recombinant expression of full-length type VII collagen and characterization of molecular mechanisms underlying dystrophic epidermolysis bullosa. J Biol Chem 2002;277(3):2118-24.

Chuai G, Ma H, Yan J, Chen M, Hong N, Xue D, et al. DeepCRISPR: optimized CRISPR guide RNA design by deep learning. Genome Biol 2018;19(1):80.

Clement K, Rees H, Canver MC, Gehrke JM, Farouni R, Hsu JY, et al. CRISPResso2 provides accurate and rapid genome editing sequence analysis. Nat Biotechnol 2019;37(3):224-6.

Concordet JP, Haeussler M. CRISPOR: intuitive guide selection for CRISPR/Cas9 genome editing experiments and screens. Nucleic Acids Res 2018;46(W1):W242-W5.

Conget P, Rodriguez F, Kramer S, Allers C, Simon V, Palisson F, et al. Replenishment of type VII collagen and re-epithelialization of chronically ulcerated skin after intradermal administration of allogeneic mesenchymal stromal cells in two patients with recessive dystrophic epidermolysis bullosa. Cytotherapy 2010;12(3):429-31.

Cox DB, Platt RJ, Zhang F. Therapeutic genome editing: prospects and challenges. Nat Med 2015;21(2):121-31.

Demeulemeester J, De Rijck J, Gijsbers R, Debyser Z. Retroviral integration: Site matters: Mechanisms and consequences of retroviral integration site selection. Bioessays 2015;37(11):1202-14.

Di WL, Larcher F, Semenova E, Talbot GE, Harper JI, Del Rio M, et al. Ex-vivo gene therapy restores LEKTI activity and corrects the architecture of Netherton syndrome-derived skin grafts. Mol Ther 2011;19(2):408-16.

Di WL, Semenova E, Larcher F, Del Rio M, Harper JI, Thrasher AJ, et al. Human involucrin promoter mediates repression-resistant and compartment-specific LEKTI expression. Human gene therapy 2012;23(1):83-90.

Doman JL, Raguram A, Newby GA, Liu DR. Evaluation and minimization of Cas9-independent off-target DNA editing by cytosine base editors. Nat Biotechnol 2020;38(5):620-8.

Droz-Georget Lathion S, Rochat A, Knott G, Recchia A, Martinet D, Benmohammed S, et al. A single epidermal stem cell strategy for safe ex vivo gene therapy. EMBO Mol Med 2015;7(4):380-93.

Fine JD, Mellerio JE. Extracutaneous manifestations and complications of inherited epidermolysis bullosa: part I. Epithelial associated tissues. J Am Acad Dermatol 2009a;61(3):367-84; quiz 85-6.

Fine JD, Mellerio JE. Extracutaneous manifestations and complications of inherited epidermolysis bullosa: part II. Other organs. J Am Acad Dermatol 2009b;61(3):387-402; quiz 3-4.

Gardella R, Belletti L, Zoppi N, Marini D, Barlati S, Colombi M. Identification of two splicing mutations in the collagen type VII gene (COL7A1) of a patient affected by the localisata variant of recessive dystrophic epidermolysis bullosa. Am J Hum Genet 1996;59(2):292-300.

Gaudelli NM, Komor AC, Rees HA, Packer MS, Badran AH, Bryson DI, et al. Programmable base editing of A*T to G*C in genomic DNA without DNA cleavage. Nature 2017;551(7681):464-71.

Georgiadis C, Rasaiyaah J, Gkazi SA, Preece R, Etuk A, Christi A, et al. Base-edited CAR T cells for combinational therapy against T cell malignancies. Leukemia 2021;35(12):3466-81.

Georgiadis C, Syed F, Petrova A, Abdul-Wahab A, Lwin SM, Farzaneh F, et al. Lentiviral Engineered Fibroblasts Expressing Codon-Optimized COL7A1 Restore Anchoring Fibrils in RDEB. J Invest Dermatol 2016;136(1):284-92.

Grocott P, Blackwell R, Weir H, Pillay E. Living in dressings and bandages: findings from workshops with people with Epidermolysis bullosa. Int Wound J 2013;10(3):274-84.

Grunewald J, Zhou R, Garcia SP, Iyer S, Lareau CA, Aryee MJ, et al. Transcriptome-wide off-target RNA editing induced by CRISPR-guided DNA base editors. Nature 2019;569(7756):433-7.

Gurevich I, Agarwal P, Zhang P, Dolorito JA, Oliver S, Liu H, et al. In vivo topical gene therapy for recessive dystrophic epidermolysis bullosa: a phase 1 and 2 trial. Nat Med 2022;28(4):780-8.

Hainzl S, Peking P, Kocher T, Murauer EM, Larcher F, Del Rio M, et al. COL7A1 Editing via CRISPR/Cas9 in Recessive Dystrophic Epidermolysis Bullosa. Mol Ther 2017;25(11):2573-84.

Hammami-Hauasli N, Kalinke DU, Schumann H, Kalinke U, Pontz BF, Anton-Lamprecht I, et al. A combination of a common splice site mutation and a frameshift mutation in the COL7A1 gene: absence of functional collagen VII in keratinocytes and skin. J Invest Dermatol 1997;109(3):384-9.

Has C, Bauer JW, Bodemer C, Bolling MC, Bruckner-Tuderman L, Diem A, et al. Consensus reclassification of inherited epidermolysis bullosa and other disorders with skin fragility. Br J Dermatol 2020;183(4):614-27.

Hou PC, Wang HT, Abhee S, Tu WT, McGrath JA, Hsu CK. Investigational Treatments for Epidermolysis Bullosa. Am J Clin Dermatol 2021;22(6):801-17.

Itoh M, Umegaki-Arao N, Guo Z, Liu L, Higgins CA, Christiano AM. Generation of 3D skin equivalents fully reconstituted from human induced pluripotent stem cells (iPSCs). PLoS One 2013;8(10):e77673.

Izmiryan A, Ganier C, Bovolenta M, Schmitt A, Mavilio F, Hovnanian A. Ex Vivo COL7A1 Correction for Recessive Dystrophic Epidermolysis Bullosa Using CRISPR/Cas9 and Homology-Directed Repair. Mol Ther Nucleic Acids 2018;12:554-67.

Jackow J, Guo Z, Hansen C, Abaci HE, Doucet YS, Shin JU, et al. CRISPR/Cas9-based targeted genome editing for correction of recessive dystrophic epidermolysis bullosa using iPS cells. Proc Natl Acad Sci U S A 2019.

Jackow J, Titeux M, Portier S, Charbonnier S, Ganier C, Gaucher S, et al. Gene-Corrected Fibroblast Therapy for Recessive Dystrophic Epidermolysis Bullosa using a Self-Inactivating COL7A1 Retroviral Vector. J Invest Dermatol 2016;136(7):1346-54.

Kern JS, Kohlhase J, Bruckner-Tuderman L, Has C. Expanding the COL7A1 mutation database: novel and recurrent mutations and unusual genotype-phenotype constellations in 41 patients with dystrophic epidermolysis bullosa. J Invest Dermatol 2006;126(5):1006-12.

Kim D, Bae S, Park J, Kim E, Kim S, Yu HR, et al. Digenome-seq: genome-wide profiling of CRISPR-Cas9 off-target effects in human cells. Nat Methods 2015;12(3):237-43, 1 p following 43.

Kim YB, Komor AC, Levy JM, Packer MS, Zhao KT, Liu DR. Increasing the genome-targeting scope and precision of base editing with engineered Cas9-cytidine deaminase fusions. Nat Biotechnol 2017;35(4):371-6.

Koblan LW, Doman JL, Wilson C, Levy JM, Tay T, Newby GA, et al. Improving cytidine and adenine base editors by expression optimization and ancestral reconstruction. Nat Biotechnol 2018;36(9):843-6.

Kocher T, Bischof J, Haas SA, March OP, Liemberger B, Hainzl S, et al. A non-viral and selection-free COL7A1 HDR approach with improved safety profile for dystrophic epidermolysis bullosa. Mol Ther Nucleic Acids 2021;25:237-50.

Kocher T, March OP, Bischof J, Liemberger B, Hainzl S, Klausegger A, et al. Predictable CRISPR/Cas9-Mediated COL7A1 Reframing for Dystrophic Epidermolysis Bullosa. J Invest Dermatol 2020;140(10):1985-93 e5.

Komor AC, Kim YB, Packer MS, Zuris JA, Liu DR. Programmable editing of a target base in genomic DNA without double-stranded DNA cleavage. Nature 2016;533(7603):420-4.

Komor AC, Zhao KT, Packer MS, Gaudelli NM, Waterbury AL, Koblan LW, et al. Improved base excision repair inhibition and bacteriophage Mu Gam protein yields C:G-to-T:A base editors with higher efficiency and product purity. Sci Adv 2017;3(8):eaao4774.

Larcher F, Dellambra E, Rico L, Bondanza S, Murillas R, Cattoglio C, et al. Long-term engraftment of single genetically modified human epidermal holoclones enables safety pre-assessment of cutaneous gene therapy. Molecular Therapy 2007;15(9):1670-6.

Latella MC, Cocchiarella F, De Rosa L, Turchiano G, Goncalves M, Larcher F, et al. Correction of Recessive Dystrophic Epidermolysis Bullosa by Transposon-Mediated Integration of COL7A1 in Transplantable Patient-Derived Primary Keratinocytes. J Invest Dermatol 2017;137(4):836-44.

Lwin SM, Syed F, Di WL, Kadiyirire T, Liu L, Guy A, et al. Safety and early efficacy outcomes for lentiviral fibroblast gene therapy in recessive dystrophic epidermolysis bullosa. JCI Insight 2019;4(11).

Ma Y, Zhang J, Yin W, Zhang Z, Song Y, Chang X. Targeted AID-mediated mutagenesis (TAM) enables efficient genomic diversification in mammalian cells. Nature methods 2016;13(12):1029-35.

Murata T, Masunaga T, Ishiko A, Shimizu H, Nishikawa T. Differences in recurrent COL7A1 mutations in dystrophic epidermolysis bullosa: ethnic-specific and worldwide recurrent mutations. Arch Dermatol Res 2004;295(10):442-7.

Naso G, Petrova A. CRISPR/Cas9 gene editing for genodermatoses: progress and perspectives. Emerg Top Life Sci 2019;3(3):313-26.

Naso G, Petrova A. Cellular therapy options for genetic skin disorders with a focus on recessive dystrophic epidermolysis bullosa. Br Med Bull 2020;136(1):30-45.

Natsuga K, Shinkuma S, Hsu CK, Fujita Y, Ishiko A, Tamai K, et al. Current topics in Epidermolysis bullosa: Pathophysiology and therapeutic challenges. J Dermatol Sci 2021;104(3):164-76.

Nystrom A, Velati D, Mittapalli VR, Fritsch A, Kern JS, Bruckner-Tuderman L. Collagen VII plays a dual role in wound healing. J Clin Invest 2013;123(8):3498-509.

Osborn MJ, Newby GA, McElroy AN, Knipping F, Nielsen SC, Riddle MJ, et al. Base Editor Correction of COL7A1 in Recessive Dystrophic Epidermolysis Bullosa Patient-Derived Fibroblasts and iPSCs. J Invest Dermatol 2020;140(2):338-47 e5.

Petrof G, Lwin SM, Martinez-Queipo M, Abdul-Wahab A, Tso S, Mellerio JE, et al. Potential of Systemic Allogeneic Mesenchymal Stromal Cell Therapy for Children with Recessive Dystrophic Epidermolysis Bullosa. J Invest Dermatol 2015;135(9):2319-21.

Petrof G, Martinez-Queipo M, Mellerio JE, Kemp P, McGrath JA. Fibroblast cell therapy enhances initial healing in recessive dystrophic epidermolysis bullosa wounds: results of a randomized, vehicle-controlled trial. Br J Dermatol 2013;169(5):1025-33.

Petrova A, Celli A, Jacquet L, Dafou D, Crumrine D, Hupe M, et al. 3D In vitro model of a functional epidermal permeability barrier from human embryonic stem cells and induced pluripotent stem cells. Stem Cell Reports 2014;2(5):675-89.

Petrova A, Georgiadis C, Fleck RA, Allison L, McGrath JA, Dazzi F, et al. Human Mesenchymal Stromal Cells Engineered to Express Collagen VII Can Restore Anchoring Fibrils in Recessive Dystrophic Epidermolysis Bullosa Skin Graft Chimeras. J Invest Dermatol 2020;140(1):121-31 e6.

Pourreyron C, Chen M, McGrath JA, Salas-Alanis JC, South AP, Leigh IM. High levels of type VII collagen expression in recessive dystrophic epidermolysis bullosa cutaneous squamous cell carcinoma keratinocytes increases PI3K and MAPK signalling, cell migration and invasion. Br J Dermatol 2014;170(6):1256-65.

Preece R, Pavesi A, Gkazi SA, Stegmann KA, Georgiadis C, Tan ZM, et al. CRISPR-Mediated Base Conversion Allows Discriminatory Depletion of Endogenous T Cell Receptors for Enhanced Synthetic Immunity. Mol Ther Methods Clin Dev 2020;19:149-61.

Ran FA, Hsu PD, Wright J, Agarwala V, Scott DA, Zhang F. Genome engineering using the CRISPR-Cas9 system. Nat Protoc 2013;8(11):2281-308.

Rees HA, Liu DR. Base editing: precision chemistry on the genome and transcriptome of living cells. Nat Rev Genet 2018;19(12):770-88.

Remington J, Wang X, Hou Y, Zhou H, Burnett J, Muirhead T, et al. Injection of recombinant human type VII collagen corrects the disease phenotype in a murine model of dystrophic epidermolysis bullosa. Mol Ther 2009;17(1):26-33.

Robertson SJ, Orrin E, Lakhan MK, O'Sullivan G, Felton J, Robson A, et al. Cutaneous Squamous Cell Carcinoma in Epidermolysis Bullosa: a 28-year Retrospective Study. Acta Derm Venereol 2021;101(8):adv00523.

Siprashvili Z, Nguyen NT, Gorell ES, Loutit K, Khuu P, Furukawa LK, et al. Safety and Wound Outcomes Following Genetically Corrected Autologous Epidermal Grafts in Patients With Recessive Dystrophic Epidermolysis Bullosa. JAMA 2016;316(17):1808-17.

Takashima S, Shinkuma S, Fujita Y, Nomura T, Ujiie H, Natsuga K, et al. Efficient Gene Reframing Therapy for Recessive Dystrophic Epidermolysis Bullosa with CRISPR/Cas9. J Invest Dermatol 2019;139(8):1711-21 e4.

Tidman MJ, Eady RA. Evaluation of anchoring fibrils and other components of the dermal-epidermal junction in dystrophic epidermolysis bullosa by a quantitative ultrastructural technique. J Invest Dermatol 1985;84(5):374-7.

Tolar J, Wagner JE. Management of severe epidermolysis bullosa by haematopoietic transplant: principles, perspectives and pitfalls. Exp Dermatol 2012;21(12):896-900.

Tsai SQ, Nguyen NT, Malagon-Lopez J, Topkar VV, Aryee MJ, Joung JK. CIRCLE-seq: a highly sensitive in vitro screen for genome-wide CRISPR-Cas9 nuclease off-targets. Nature methods 2017;14(6):607-14.

Tsai SQ, Zheng Z, Nguyen NT, Liebers M, Topkar VV, Thapar V, et al. GUIDE-seq enables genome-wide profiling of off-target cleavage by CRISPR-Cas nucleases. Nature biotechnology 2015;33(2):187-97.

Venugopal SS, Yan W, Frew JW, Cohn HI, Rhodes LM, Tran K, et al. A phase II randomized vehicle-controlled trial of intradermal allogeneic fibroblasts for recessive dystrophic epidermolysis bullosa. J Am Acad Dermatol 2013;69(6):898-908 e7.

Wagner JE, Ishida-Yamamoto A, McGrath JA, Hordinsky M, Keene DR, Woodley DT, et al. Bone marrow transplantation for recessive dystrophic epidermolysis bullosa. The New England journal of medicine 2010;363(7):629-39.

Webber BR, Osborn MJ, McElroy AN, Twaroski K, Lonetree CL, DeFeo AP, et al. CRISPR/Cas9-based genetic correction for recessive dystrophic epidermolysis bullosa. NPJ Regen Med 2016;1.

Wilson LOW, O'Brien AR, Bauer DC. The Current State and Future of CRISPR-Cas9 gRNA Design Tools. Front Pharmacol 2018;9:749.

Woodley DT, Keene DR, Atha T, Huang Y, Lipman K, Li W, et al. Injection of recombinant human type VII collagen restores collagen function in dystrophic epidermolysis bullosa. Nat Med 2004;10(7):693-5.

Woodley DT, Wang X, Amir M, Hwang B, Remington J, Hou Y, et al. Intravenously injected recombinant human type VII collagen homes to skin wounds and restores skin integrity of dystrophic epidermolysis bullosa. J Invest Dermatol 2013;133(7):1910-3.

Ye K, Schulz MH, Long Q, Apweiler R, Ning Z. Pindel: a pattern growth approach to detect break points of large deletions and medium sized insertions from paired-end short reads. Bioinformatics 2009;25(21):2865-71.

FIGURE LEGENDS

Figure 1. Experimental design for cytosine base editing for the correction of a *COL7A1* mutation

a. Schematic of codon optimized cytosine base editor (coCBE3) protein structure and mechanism of action. Rat apolipoprotein B mRNA editing enzyme (rAPOBEC1) links to Streptococcus pyogenes Cas9 D10A nickase (nCas9) and a uracil glycosylase inhibitor (UGI) domain to prevent excision and reversion of U:G mismatches. NLS indicated nuclear localisation signal (NLS). Following Cas9 binding, rAPOBEC1 mediates C-to-U conversion by deamination of single-stranded DNA displaced by the protospacer within a 5BP editing window corresponding to the 4th and 8th nucleotides 5' of the protospacer. **b.** Schematic showing the x3C7-CyD guide RNA designed to target exon3/intron3 junction of *COL7A1* at position C5 (antisense) corresponding to the c.425A>G RDEB point mutation highlighted in red. Dotted lines show coCBE3 activity window. Below Sanger-sequencing traces confirming the presence of homozygous c.425A>G mutation in human fibroblasts (top) and iPSCs (bottom). **c.** RDEB fibroblasts were isolated and reprogrammed into iPSC. Both cell types were then gene edited by electroporation of coCBE3 mRNA and x3C7-CyD sgRNA. Functional C7 recovery from base edited fibroblasts was assessed *in vivo* using a human:murine xenograft skin model. Corrected iPSCs were differentiated towards keratinocyte-like cells to assess C7 restoration *in vitro*.

Figure 2: Characterization of patient-derived RDEB iPSCs.

a. *In situ* immunofluorescence staining for pluripotency markers. From left to right: Sox2, SSEA-4 and Oct3/4. Nuclei were counterstained with DAPI (blue). Wild-type (WT) iPSCs were used as a positive control. Scale bar = 50μm. **b.** Representative quantification of pluripotency-associated markers by flow cytometry for RDEB (top) and WT (bottom) iPSCs.

c. Confirmation of expression of NANOG, Sox2, Oct4, KFL4, cMYC pluripotency markers in RDEB (top) and WT (middle) iPSCs by RT-PCR. RDEB fibroblasts were used as a negative control (bottom). **d.** RDEB iPSCs are able to differentiate towards all three germ layers as shown by their expression of TUBB3 (ectoderm), αSMA (mesoderm), and AFP (endoderm) in trilineage differentiation assay.

Figure 3. Confirmation of efficient base editing in patient fibroblasts and iPSCs

a. Sanger sequencing and EditR analysis of base edited RDEB fibroblasts (left) and iPSCs (right). The base editing window is boxed in blue, the desired base change at position C5 (c.425) is boxed in red. Histogram legend: black- G, green- A, blue- C, red- T. Substitution rate at each position of the x3C7-CyD protospacer is shown in the table. 61% and 45% of targeted C>T (G>A) conversion was detected in patient fibroblasts and iPSCs, respectively. Bystander C>T conversions at position C4 were detected in 8% and 4% in patient fibroblasts and iPSCs, respectively. **b.** NGS analysis of CBE3 activity in patient fibroblasts (left) and iPSCs (right) showing C>T conversion across the protospacer with the C positions indicated below. 59.6% and 51% of the targeted c.425A>G mutation correction was detected in patient iPSCs and fibroblasts, respectively (green bar). On-target bystander C>T conversions were detected at position C4 (4.82% and 19.39% in patient fibroblasts and iPSCs, respectively) and outside the base editing window at position C3 (3.89% and 1.01% and 3.89% in patient fibroblasts and iPSCs, respectively), C1 (7.44%inpatient iPSCs only) and C12 (1.03% in patient iPSCs only). **c.** CRISPResso2-based haplotype quantification of NGS data in base edited fibroblasts (left) and iPSCs (right). The percentage of reads with a correction at position c.425 alone is shown by the green bar (46% and 23.55% in patient fibroblasts and iPSCs, respectively). Bystander C>T edits and non C>T base changes are shown within the 5bp coCBE3 deamination activity window in exon 3 of *COL7A1* (upper case letters, dotted box) and outside the base editing

window within the exon 3 splicing donor (SD) sequence of *COL7A1* (lower case letters, highlighted in gray).

Figure 4. Targeted base editing of a *COL7A1* mutation and potential guide directed off target sites

a. Top 10 off-target sites for x3C7-CyD sgRNA predicted by Benchling and are shown in column 1. Highlighted in red are mismatch bases between the off-target site and the *COL7A1* x3C7-CyD sgRNA target (column 2). For each predicted off-target, gene name and relative location within coding or noncoding sites is indicated in column 3. **b.** A plot showing coCBE3-mediated C>T conversions within the base editing window of *COL7A1* and off-target sites for untreated (unt) and treated samples (coCBE3). **c.** A plot showing percentages of insertions and deletions (indels) for *COL7A1* and off-target sites for untreated (unt) and treated samples (coCBE3).

Figure 5. Base editing restores C7 expression *in vitro* in fibroblasts and iPSC-derived keratinocyte-like cells.

a. Restoration of C7 (green) expression in base edited fibroblasts by immunofluorescence staining. Untreated RDEB fibroblasts and wild type fibroblasts were used as a negative and positive controls, respectively. Scale bar = 50 μm. **b.** C7 western blotting from cell lysate confirms the presence of full-length (~290 kDa) C7 in base edited fibroblasts. No C7 expression was observed in untransduced cells. Lenti-C7 transduced fibroblasts and wild type fibroblasts were used as positive controls. Vinculin was used as loading control. **c.** C7 western blotting using cell culture supernatant confirms that base edited fibroblasts are able to secrete functional, full-length C7. No secreted C7 was detected in untreated RDEB fibroblasts. Lenti-C7 transduced fibroblasts and wild type fibroblasts were used as positive controls. Ponceau S staining was used as a loading control. **d.** Left: Phase contrast image of base edited iPSC-

derived keratinocyte-like cells showing typical epidermal cell morphology. Middle: iPSC-derived keratinocyte-like cells co-expressing epidermal stem cell markers, △Np63 (red) and K14 (green). Right: iPSC-derived keratinocyte-like cells express *de novo* C7 (green). △Np63 expression is shown in red. Scale bar = 50 μm. RDEB FBs unt- untreated RDEB fibroblasts, RDEB coCBE3 FB- base edited fibroblasts, WT FBs- wild-type fibroblasts, LV-coC7- RDEB fibroblasts transduced with lentiviral vector containing codon optimised *COL7A1*, L- ladder.

Figure 6. Human skin equivalents produced using base edited fibroblasts display normal epidermal morphology and stratification.

a. H&E staining demonstrates normal morphology of human skin. Blistering shown by the black arrow. Scale bar = 60 μm. **b.** Human origin of the graft was confirmed by human specific Cytochrome C oxidase (Complex IV) subunit II (MTCO2) staining (red). White dotted line demarcates the border between mouse and human tissue. **c.** Immunofluorescent staining for Keratins 14 (red) and 10 (green) showed normal differentiation pattern of the grafts with basal expression of the former and suprabasal localization of the latter. Scale bar = 50 μm. WT- wild type grafts, RDEB unt- untreated RDEB grafts, RDEB CBE FB- grafts containing base edited fibroblasts and untreated RDEB keratinocytes, hu- human, ms- mouse.

Figure 7. *In vivo* functional correction through type VII collagen deposition and *de novo* anchoring fibril (AF) formation.

a. Immunofluorescent analysis of C7 (green) expression at the dermal-epidermal junction (DEJ). Strong C7 expression can be seen throughout the DEJ of healthy grafts (left), whereas it is completely absent in RDEB grafts (middle). Robust, albeit patchy C7 expression can be detected in the grafts containing base edited fibroblasts. Inserts show the magnified view of the DEJ. Scale bar = 50 μm. **b.** TEM analysis of the skin grafts shows the formation of *de novo* anchoring fibrils (AFs). Images are shown at the following magnification: x2000, scale

bar=2μm, x15,000, scale bar=500nm and x30,000, scale bar=200nm. Green arrows point at AFs. Black stars show blister. **c.** Quantitative analysis revealed significantly higher density of AFs in grafts containing base edited fibroblasts compared to untreated RDEB grafts. Statistical analysis carried out using Student's t-test. Error bars represent standard deviation (SD) n=3 for each condition. WT- wild type grafts, RDEB unt- untreated RDEB grafts, RDEB CBE FB- grafts containing base edited fibroblasts and untreated RDEB keratinocytes, KC- keratinocyte, DEJ- dermal-epidermal junction.

Figure 8: Representative images of C7 expression by immunofluorescence and AF formation by TEM.

a. and **c.** Immunofluorescent analysis of C7 (green) expression at the dermal-epidermal junction (DEJ). Strong C7 expression can be seen throughout the DEJ of healthy grafts (left), whereas it is completely absent in RDEB grafts (middle). Robust, albeit patchy (**a**) or continuous, dim (**c**) C7 expression can be detected in the grafts containing base edited fibroblasts. Inserts show the magnified view of the DEJ. Scale bar =50μm. **b.** and **d**. Representative TEM images of the grafts shown in **a.** and **c.** *De novo* AFs formation was detected in grafts containing base edited fibroblasts, while no fully formed AFs were observed in untreated grafts. Images are shown at the following magnifications x15,000, scale bar=500nm and x30,000, scale bar=200nm. Green arrows point at AFs. WT- wild type grafts, RDEB unt- untreated RDEB grafts, RDEB CBE FB- grafts containing base edited fibroblasts and untreated RDEB keratinocytes, KC- keratinocyte, DEJ- dermal-epidermal junction.

Table 1: Next generation sequencing data analysis of top 10 guide-dependent off-target sites. Percentage C>T conversion in CBE3 or UT (untreated) samples across C bases within each 20 bp off-target sequence. CBE3-activity window is highlighted in bold.

Gene	C position	% base conversion	
		UT	CBE
C7 ON	1	0.00	0.78
	3	0.18	1.01
	4	**0.45**	**4.08**
	5	**5.82**	**59.62**
	12	0.00	0.15
	14	0.00	0.1
	15	0.09	0.15
	20	0.09	0.05
C7 OT1	3	0.02	0.07
	4	**0.05**	**0.00**
	5	**0.04**	**0.01**
	12	0.00	0.01
	14	0.05	0.05
	15	0.09	0.02
	20	0.03	0.01
C7 OT2	1	0.08	0.09
	3	0.09	0.05
	4	**0.06**	**0.09**
	5	**0.03**	**0.07**
	12	0.08	0.04
	14	0.05	0.07
	15	0.07	0.04
	20	0.02	0.00
C7 OT3	3	0.00	0.02
	4	**0.00**	**0.49**
	5	**0.10**	**4.09**
	12	0.05	0.19
	14	0.00	0.02
	15	0.05	0.00
	20	0.20	0.02
C7 OT4	1	0.00	0.00
	3	0.00	0.00
	4	**0.01**	**0.00**
	5	**0.00**	**0.00**
	12	0.00	0.01
	15	0.03	0.00
C7 OT5	1	0.15	0.18
	3	0.10	0.06

	4	**0.11**	**0.12**
	5	**0.02**	**0.02**
	12	0.00	0.06
	15	0.00	0.05
	20	0.09	0.00
C7 OT6	**4**	**0.13**	**0.15**
	5	**0.00**	**0.03**
	12	0.00	0.00
	14	0.00	0.00
	15	0.03	0.06
C7 OT7	3	0.09	0.00
	4	**0.09**	**0.00**
	5	**0.00**	**0.21**
	11	0.00	0.00
	12	0.05	0.00
	14	0.00	0.00
	15	0.10	0.00
	19	0.10	0.00
	20	0.00	0.11
C7 OT8	3	0.01	0.04
	4	**0.00**	**0.00**
	5	**0.00**	**0.00**
	12	0.03	0.00
	14	0.03	0.00
	15	0.03	0.00
	19	0.04	0.01
	20	0.04	0.07
C7 OT9	1	0.06	0.00
	3	0.00	0.00
	4	**0.00**	**0.00**
	5	**0.06**	**0.00**
	12	0.06	0.00
	14	0.00	0.00
	15	0.00	0.00
	19	0.00	0.21
	20	0.06	0.00
C7 OT10	1	0.03	0.02
	3	0.00	0.06
	4	**0.02**	**0.00**
	5	**0.00**	**0.04**
	12	0.03	0.05
	15	0.02	0.02
	20	0.00	0.03

Table 2. Top 10 *in silico* predicted sites interrogated by NGS.

Off-target	Sequence	PAM	Chromosome	Strand	Position
C7-ON	CACCCTGGGGACACCAGGTC	GGG	chr3	-1	48593551
C7-OT1	TACCCTGGGGGCACCAGGTC	CAG	chr10	-1	71798536
C7-OT2	CACCCTGGAGACACCAGGAC	TAG	chr19	-1	19637825
C7-OT3	GACCCTGGGTACACCAGGTC	AGG	chr5	1	65716931
C7-OT4	CACCCTGGGGACAGCAGGTA	GGG	chr6	1	161111959
C7-OT5	CACCCTGGGGACAGCATGTC	CAG	chr16	1	88952889
C7-OT6	GAGCCTGGGGACACCAGGTG	CAG	chr12	-1	5873281
C7-OT7	GACCCTGGGGCCACCAGGCC	AGG	chr7	1	149729342
C7-OT8	AACCCTGGGAACACCAGGCC	AAG	chr17	1	31512778
C7-OT9	CTCCCTGGGGTCACCAGGCC	GAG	chr17	1	76982342
C7-OT10	CTCCCTGGGGACATCAGGGC	TGG	chr1	-1	6337136

Table 3. Primer sequences for NGS library preparation. Primers are given in the 5'-3' orientation. Fwd: forward, Rev: reverse

Primer name	Sequence
C7-ON FWD	CGGTTCCCCTGGACACTT
C7-ON REV	ACAGGACAGAGTTCGGCC
C7-OT1 FWD	TACGCCCCAGTTCAAGCC
C7-OT1 REV	AGGGGCTGTGGTCTCTCT
C7-OT2 FWD	AGGCATGGTCAGAGCAGG
C7-OT2 REV	CCAAGCAGCGAATCGTGT
C7-OT3 FWD	AAAGGTCTGGGCTGAGGG
C7-OT3 REV	TGGTCAGTTCTCAGCTTTCAT
C7-OT4 FWD	AATGCCCAGACCATGCCT
C7-OT4 REV	AGCCCAAGTGTGTGAGGA
C7-OT5 FWD	CCCCATGACAGCCCATCA
C7-OT5 REV	TCAGCAGCAAACCCGATG
C7-OT6 FWD	GAGTGAGGGCTGAGCAGT
C7-OT6 REV	TTGCCCACAGAGTCCCAG
C7-OT7 FWD	CAGGACTGAGGGCTGAGG
C7-OT7 REV	GTCAGTACCGAGGGCAGG
C7-OT8 FWD	GGCTCTGGGTCTTGAGGG
C7-OT8 REV	CCAGGGCAGCTTCCAAGA
C7-OT9 FWD	ACAGAGAGGCAGCCGAAG
C7-OT9 REV	CTGCTTCCCCTGCCAGAA
C7-OT10 FWD	TCCTGCCTTCTCCAAGCC
C7-OT10 REV	AGCATGAGAGAGCAGCCC

Table 4: List of antibodies used in this study.

Target	**Company**	**Application**
Monoclonal Anti-Collagen Type VII, LH7.2 clone	Sigma-Aldrich	Immunofluorescence
Polyclonal Anti- Collagen Type VII	Gift from Prof Chen	Immunoblotting
Polyclonal Anti-Keratin 14	BioLegend	Immunofluorescence
Monoclonal Anti-Keratin 10	Abcam	Immunofluorescence
Monoclonal Anti-Human Cytochrome C oxidase (Complex IV) subunit II	Abcam	Immunofluorescence
Monoclonal Anti-Vinculin	Sigma-Aldrich	Immunoblotting
Anti SOX2-human-FITC	Miltenyi Biotech	Flow cytometry
Anti NANOG-human APC	Miltenyi Biotech	Flow cytometry
Anti TRA 1-60-human PE	Miltenyi Biotech	Flow cytometry
Anti TRA 1-81-human PE	Miltenyi Biotech	Flow cytometry
Anti SSEA-4-human PE	Miltenyi Biotech	Flow cytometry
Polyclonal Anti-SOX2	Sigma-Aldrich	Immunofluorescence
Monoclonal Anti-OCT-3/4	Santa Cruz Biotech	Immunofluorescence
Monoclonal Anti-AFP	Sigma-Aldrich	Immunofluorescence
Monoclonal Anti-ACTA2	Sigma-Aldrich	Immunofluorescence
Monoclonal Anti-TUBB3	Sigma-Aldrich	Immunofluorescence
Monoclonal Anti-ΔNp63	Abcam	Immunofluorescence

Figure 1

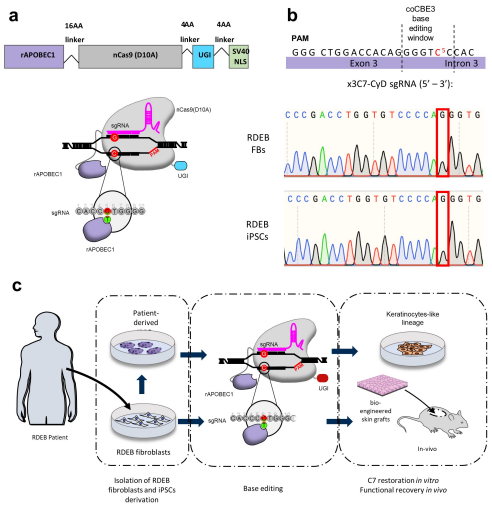

Figure 2

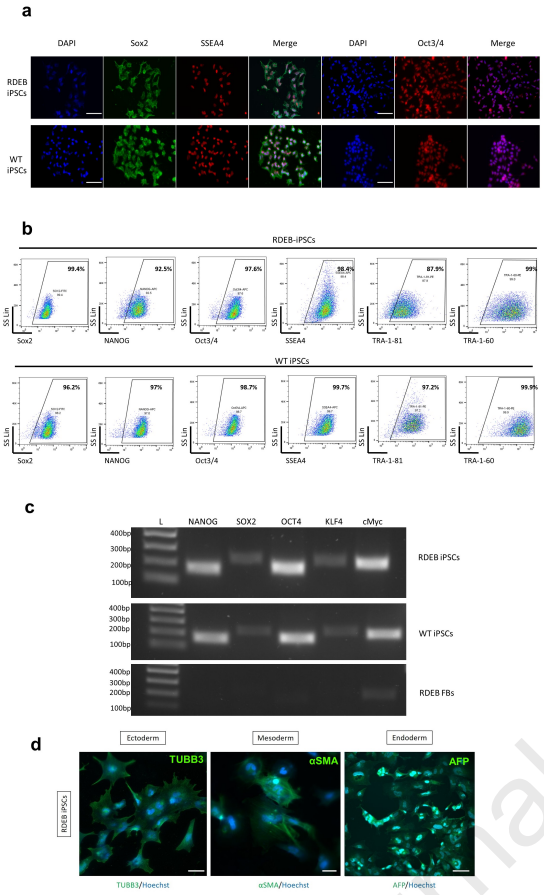

Figure 3

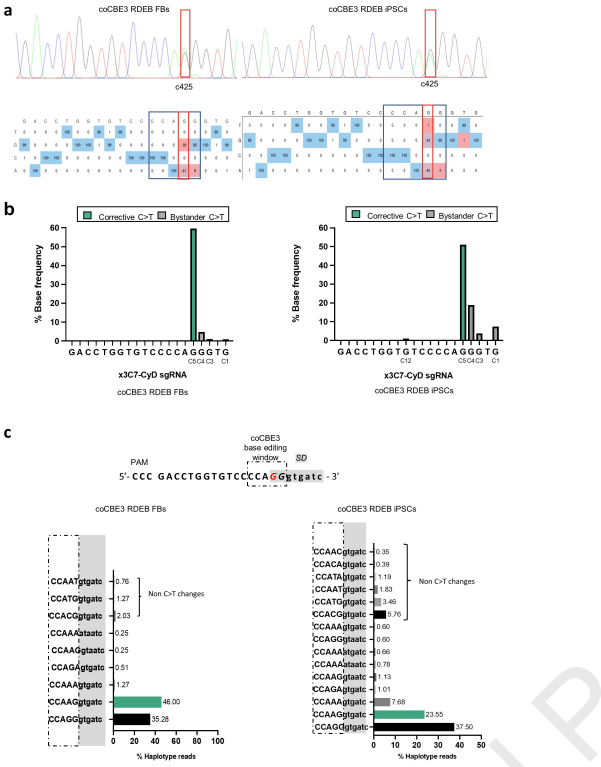

Figure 4

a

Target	gRNA sequence	Gene
COL7A1	CACCTTGGGGACACCAGGTC	*COL7A1*
OT1	TACCCTGGGGGCACCAGGTC	Exon 3, *CDH23*
OT2	CACCCTGGAGACACCAGGAC	Intron 10, *GMIP*
OT3	GACCCTGGGTACACCAGGTC	Intron 2, SGTB
OT4	CACCCTGGGGACAGCAGGTA	Exon 24, *MAP3K4*
OT5	CACCCTGGGGACAGCATGTC	Intron 1, *CBFA2T3*
OT6	GAGCCTGGGGACACCAGGTG	Intron 3, *ANO2*
OT7	GACCCTGGGGCCACCAGGCC	Exon 14, *KRBA1*
OT8	AACCCTGGGAACACCAGGCC	Intron 3, *RAB11FIP4*
OT9	CTCCCTGGGGTCACCAGGCC	Intergenic, Chr17
OT10	CTCCCTGGGGACATCAGGGC	Intron 3, *ACOT7*

b

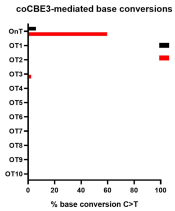

c

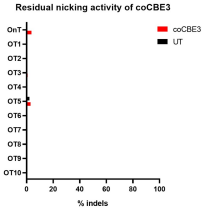

Figure 5

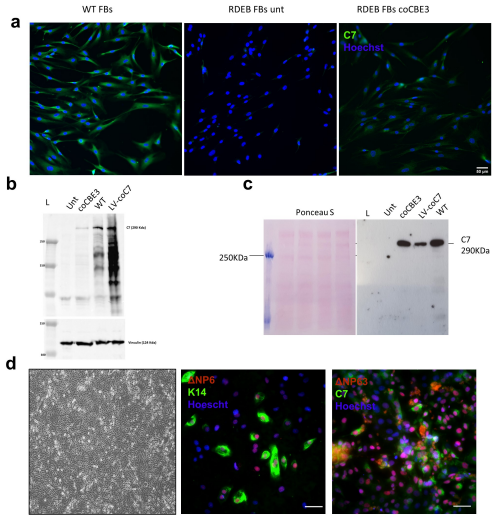

Figure 6

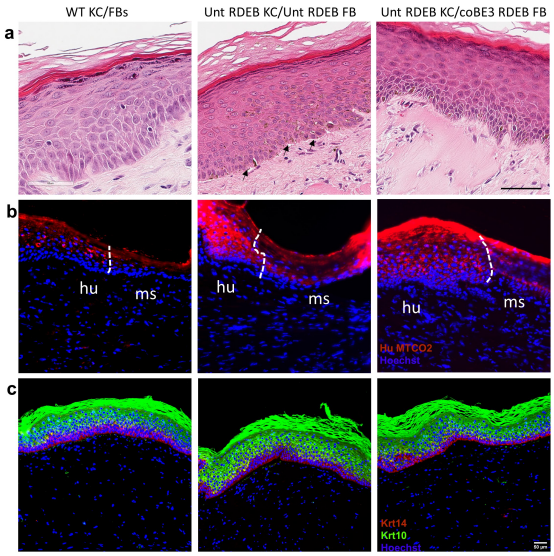

Figure 7

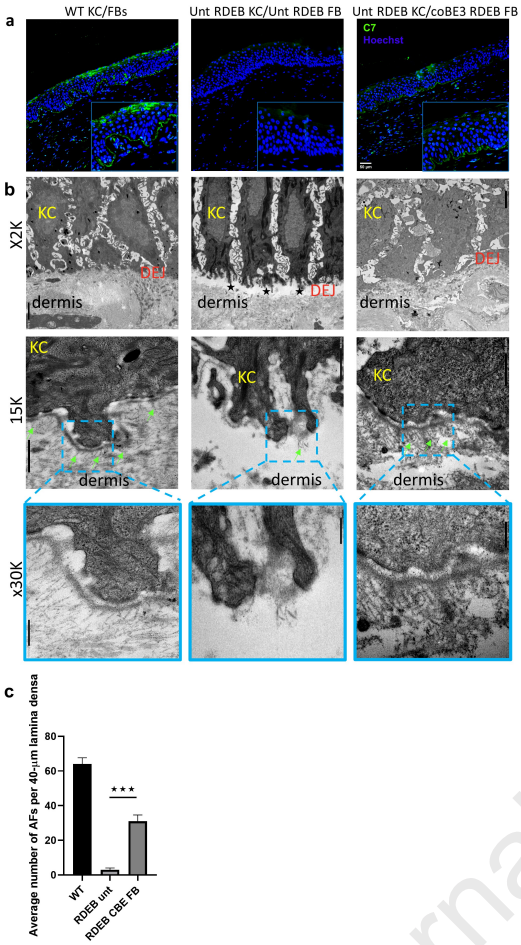

Figure 8